International Journal of Civil Engineering (2023) 21:789–804
https://doi.org/10.1007/s40999-022-00802-4

RESEARCH PAPER

Experimental and Numerical Investigation of the Structural, Thermal and Acoustic Performance of Reinforced Concrete Slabs with Balls for a Cleaner Environment

Musa Hakan Arslan[1] · Yasin Onuralp Özkılıç[2] · H. Derya Arslan[3] · Ömer Sinan Şahin[4]

Received: 15 July 2022 / Revised: 24 December 2022 / Accepted: 28 December 2022 / Published online: 18 January 2023

Abstract

This study conducted a comprehensive experimental and numerical assessment to investigate the effect of plastic circular balls placed in the middle of a section of a reinforced concrete slab on strength, ductility, thermal, and acoustic performance. The ball diameter/slab thickness (D/H), grades of concrete, and longitudinal tensile reinforcement ratio (ρ) in the slab were selected as the main variables. The variation in thermal and acoustic performance depending upon the ball's diameter was investigated as well. The results showed that the slab's load-carrying capacity, ductility, and energy dissipation capacity did not differ if the D/H ratio did not exceed 0.4; however, significant decreases in these values were observed when the D/H ratio exceeded 0.4. Moreover, the increase in the concrete and reinforcement's strength had a negative effect on the slab with a D/H ratio of 0.8. The experimental results revealed that balled slabs are 3.15 times superior with respect to thermal conductivity and provide 1.38 times more insulation to absorb sound compared to non-balled slabs. In the numerical study of the slabs' thermal performance, the mean surface temperature and heat flux on the slab where the heat transfer takes place decreased as the ball diameter increased. As seen in acoustic models, the level at which the slabs absorbed sound varied depending upon both the diameter of the balls and the sound frequency.

Keywords Slab tests · Ball · Finite element model · Thermal tests · Acoustic tests

1 Introduction

For architectural reasons and ease of application, flat slabs are preferred in many reinforced concrete (RC) buildings. However, the slabs are quite thick, which is a significant problem particularly in buildings with large slab spans. This situation increases the amount of concrete material used in the building, as well as the building's weight, its foundation's dimensions, and the earthquake force that will affect the structure.

Reducing the cost of concrete made with natural resources and the damage to the environment is an extremely important issue. The advantages of limiting the natural resources used in concrete production have been discussed, particularly from the perspective of sustainable design [1–3]. This issue is much more critical in economically developing countries such as Turkey, where the risk of earthquakes is high and the population is increasing rapidly.

✉ Musa Hakan Arslan
mharslan@ktun.edu.tr

Yasin Onuralp Özkılıç
yozkilic@erbakan.edu.tr

H. Derya Arslan
deryaarslan@erbakan.edu.tr; kolderya@hotmail.com

Ömer Sinan Şahin
ossahin@ktun.edu.tr

[1] Department of Civil Engineering, Faculty of Engineering and Natural Sciences, Konya Technical University, 42250 Konya, Turkey

[2] Department of Civil Engineering, Faculty of Engineering, Necmettin Erbakan University, 42100 Konya, Turkey

[3] Department of Architecture, Fine Art and Architecture Faculty, Necmettin Erbakan University, 42100 Konya, Turkey

[4] Department of Mechanical Engineering, Faculty of Engineering and Natural Sciences, Konya Technical University, 42250 Konya, Turkey

Apart from these concerns, in addition to a building's mechanical performance (such as sufficient strength, rigidity, and ductility) during its service life, it is also extremely important to provide comfort for its occupants. For example, sufficient thermal and sound insulation in a building are important indoor comfort conditions [4–6]. Reinforced concrete (RC) slabs, which are one of the RC members with the highest thermal and sound transmission, are very important in this respect. This situation has been discussed in different disciplines in recent years, and different solutions have been developed to increase RC members' insulation capacity [7, 8].

Because of the issues aforementioned, the research on innovative materials and technologies that both improve a building's performance under loads, lighten the structure, and have more positive attributes with respect to thermal-sound insulation is still continuing in the construction of RC buildings. It has been found that one of the most effective solutions to the problems above is to use plastic balls (spacers) in an RC building's slabs [9]. It is necessary for these voids to be as circular or elliptical as possible to prevent stress concentrations that will occur in the section [10].

Although there have been many experimental studies [11–13] on the bending and punching performances of circular plastic voids on flat slabs, these studies focused on very limited parameters. The numerical outcomes indicated that the finite element analysis (FEA) results [14–25] showed a good correlation for the slabs with experimental results.

An experimental study was conducted first to observe the effect of plastic circular void formers (balls) placed in the middle of the section on the slab's mechanical behavior, and then the results obtained from the experimental study were modeled with finite element using ABAQUS and ANSYS software and the results were verified. As there are no comprehensive parametric studies in the literature, the main parameters that can affect the slab's performance—different levels of void (ball) diameter/slab thickness (D/H), concrete grades, and longitudinal tensile reinforcement ratio (ρ) in the slab—were selected. A comprehensive analysis was carried out on 24 finite element models (FEM). In addition to the behavior under vertical loads of slabs with and without balls, the variation in thermal and acoustic performance depending upon the balls' diameter was investigated both experimentally and numerically. The analysis results related to thermal and acoustic performance were interpreted based upon balls of different diameters, similar to the parametric study in vertical loading.

2 Theoretical Background

Concrete, which has been used as a building material since the 1990s, is a man-made stone. A significant part of the material in the concrete (between 70 and 80%) is aggregate that is obtained from natural resources [1]. To reduce in part the environmental damage attributable to concrete production, different alternatives to using aggregate have been studied [26–30]. The most popular of these are the use of recycled aggregates, solid waste, and plastic materials. When these materials are used in the concrete in the appropriate ratio, there is an improvement in the concrete's tensile strength, but the compressive strength is generally not at the levels desired. Another important point in the use of such materials is the material mixture's homogeneity, as the distribution of these materials in the concrete may not be homogeneous. Therefore, RC elements may lose strength where these materials are used, and thus, it is extremely important that these materials that are used to lighten the concrete are used as much as possible in the region where they will not be required statically.

In addition to the environmentally sensitive new generation measures that can be taken during concrete production, limiting the use of concrete in areas that are unnecessary in the production of structural elements is also very popular, as it reduced the cumulative use of concrete. The use of concrete in RC slabs is limited with plastic circular void formers, which have been applied widely, particularly in Europe (Fig. 1). Many firms (U-BOOT Beton, Cobiax, and The Bubble Deck) are still conducting research on this subject [31–34] and are developing the expertise needed to reduce the volume of concrete used, particularly in slabs.

It is known that plastic voids reduce the moment carrying capacity less, particularly in bending elements such as slabs, but cause a considerable decrease in strength because of the loss of the cross-sectional area in shear active elements [35, 36]. Accordingly, it is common to use plastic void formers in the bending region. However, there are limitations and reservations about punching damage (which is brittle shear damage) around the column in flat slabs. As a result of these studies, it has been predicted that these materials (plastic void formers or balls) can reduce the concrete used by approximately 30%, particularly in large-span slabs, if the slabs' heights approach 50 cm. Figure 1 shows the schematic view of a slab with balls and an example of this type of slab application in the USA. Further, there are also a number of green attributes that Suzan et al. [37] described, including lower energy consumption and a reduction in CO_2 emissions, which make balls more environmentally friendly than other concrete construction techniques.

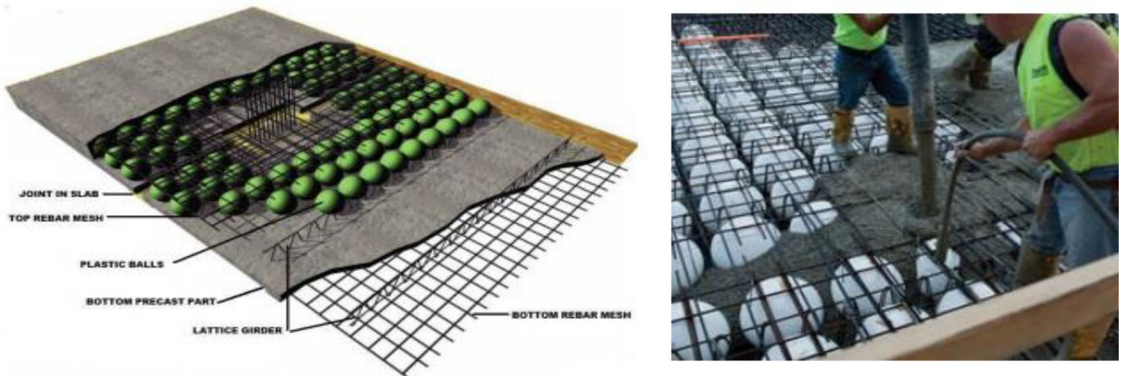

Fig. 1 Structure of Balled Slab (https://www.cobiax.com/intl/en/)

In a section subjected to bending, which is one of the simple strength states, there is no theoretical need for the material in the neutral axis region where the stress is very low. Therefore, the narrowing in the middle of the section or the gaps created in most carrier system elements (such as large-span beams) do not lead to any weakness in behavior. On the contrary, because it reduces the carrier system's weight, it reduces the carrier elements' load/capacity ratio. Therefore, the concrete savings in these regions make an important contribution.

In RC structures, the slab elements are generally under the effect of bending, except for the regions where the slab connects to the column. The shear force (V_d) on the slab is often much less than the shear force (V_{cr}) that only the concrete will bear. The shear failure in RC flat slabs occurs particularly when the tensile stress exceeds the limit value. As these failures are sudden, their effects are destructive. The high axial load that is transferred from the columns in flats slabs can cause shear failure in the slabs. Many methods can be applied to prevent this failure, such as increasing slab thickness in the area adjacent to the column, increasing column thickness, which is contrary to the architectural desire, increasing the concrete's tensile strength, providing a slab with shear reinforcement, etc. However, unlike conventional slabs, the punching effect is much more critical because of the structural placement of balled slabs. The experimental results in the literature [14] have shown as well that the shear resistance of a slab with plastic balls is 60% of that of the traditional slab with the same thickness. In addition, the test results in punching estimation studies [38–40] have shown that the punching shear estimates of the building codes are quite inconsistent for balled slabs. Therefore, it is necessary to apply different equations for punching in these slabs' design. The most effective way to avoid the punching problem is not to place the balls around the column (which can be at least twice the slab's thickness) and additional vertical reinforcement in the shear section can be provided to solve this problem.

When the RC building stock in Turkey (and similar countries) is analyzed, flat slabs' preferred thickness is 12–30 cm based upon the loads and span length; therefore, the ball radius must be smaller than the radius that European construction firms use commonly. Compared to European countries, there is a need for more multi-story RC structures in countries such as Turkey because of the rapid population increases attributable to immigration and the younger population. As a result, tests must be performed with balls of smaller diameters.

3 Slab Experiments: Loading Test

The experimental study, which investigated slabs' load carrying, ductility, and energy absorption capacities, was carried out on two different RC slabs. One was produced as a reference specimen without balls, while the other had plastic spacers. In the experimental stage of the study, all of the full geometric scale RC slabs were tested first under vertical loading (four-point flexural test) in Konya Technical University Structure and Earthquake Laboratory, as shown in Fig. 3. The slab thickness chosen was 150 cm and those without balls were referred to as F_1 and those with balls were referred to as F_2.

The slab elements' dimensions (length/width/height) were 2100/1000/150 mm. TBC-500-2000 [41] maximum deflection conditions were taken into account in the selection of the slabs' thickness. Steel reinforcements were chosen at a rate of 0.6% (7 Ø 12) to create under-balanced behavior in slabs where the cover thickness was chosen as 30 mm. In the TBC-500-2000, the minimum bar ratio is given as 0.002 for one-way slabs.

The ratio of the lower and upper longitudinal reinforcement bars used in the slabs was the same. In the experiments, the average 28-day 150/300 mm cylinder compressive strength used in concrete production was found to be 25.96 MPa, while a strength of 1.32 MPa was

Table 1 Concrete Mix Proportion for Slabs (weight for 1 m^3 of concrete)

Material	F_1 and F_2	
	Weight (N)	Proportion (%)
Cement (grade 42.5)	4300	17.4
Aggregate-1 (0–4 mm)	10,400	42.1
Aggregate-2 (4–7 mm)	7950	32.2
Water	1935	7.8
Admixture (Sika HE-200)	86	0.3
Total	24,670	100

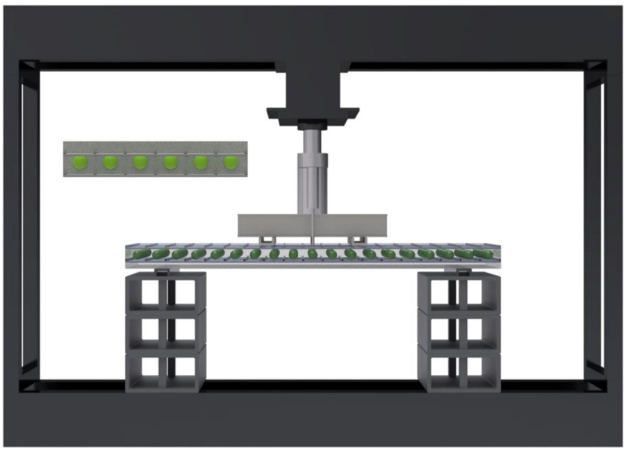

Fig. 2 The test set-up and schematic view of the specimen

obtained in the splitting tests. The average yield strength of the longitudinal reinforcement used was approximately 525 MPa. The amounts of the concrete mixture are presented in Table 1. In each series of casting, the specified compressive strength was measured by testing cylinders with three dimensions.

The diameter selected for the plastic balls was 6 cm, and the cross section of a typical section is shown in Fig. 2. The balls replaced the neutral axis of the sections of the slab. As shown in the figure, plastic spacers with a diameter of 60 mm were chosen. This selection was made to be 40% of the section's total height. As depicted in Fig. 2, with the help of steel wires, the balls were connected to the area where the tension was theoretically absent and their

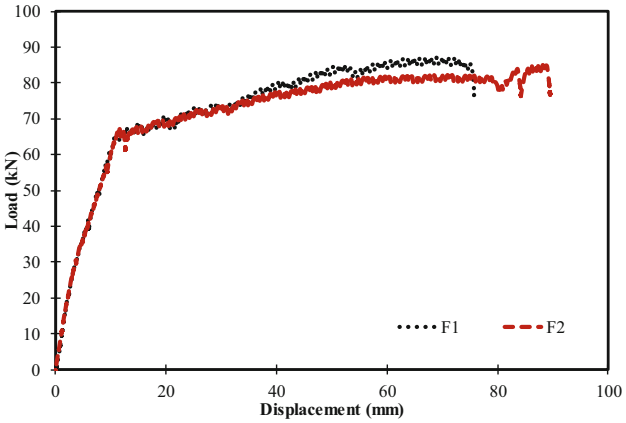

Fig. 3 Load–displacement capacity curves of the slabs

positions remained constant when the concrete was poured. The greatest problem in this type of production is keeping the axes of the balls and the neutral axis regions as close as possible. Therefore, the wires connected to the mold ends were passed through the balls and the balls were suspended. The number of balls per square meter was approximately 54. The plastic ball's characteristics are given in Table 2.

Slabs were tested in a four-point bending test set-up under a one-way increasing vertical load in a loading set-up with a capacity of approximately 500 kN. A spreader beam was placed on the specimens symmetrically with a support gap of 650 mm, and the load was applied to the center of the beam. The distance between the spreader beam' support and the closest beam support was 650 mm. Measurements were recorded electronically with high-precision data measuring devices and transferred to the computer. The load was applied until yielding with an increasing loading of 10 kN. Linear displacement gages (LVDT) were placed in the lower part of the beam to measure displacement. The test apparatus and a schematic view of the specimens are shown in Fig. 2.

Figure 3 shows vertical load and vertical displacement graphs of the samples. After the load was controlled (in 10 kN increments) to the yielding moment (the yielding in the longitudinal reinforcement was observed during the test after the load capacity was reached), loading with a displacement increment (10 mm) was applied. As the curves show, the load-carrying capacities of the slabs with and

Table 2 Plastic ball characteristics

Diameter (cm)	Thickness (cm)	Unit weight of plastic (g/cm^3)	Distance between ball axes (cm)	The number of balls in slabs	Volumetric ratio $V_{ball}/V_{slab\ (full)}$
6.00	0.14	1.2	110	114	0.327

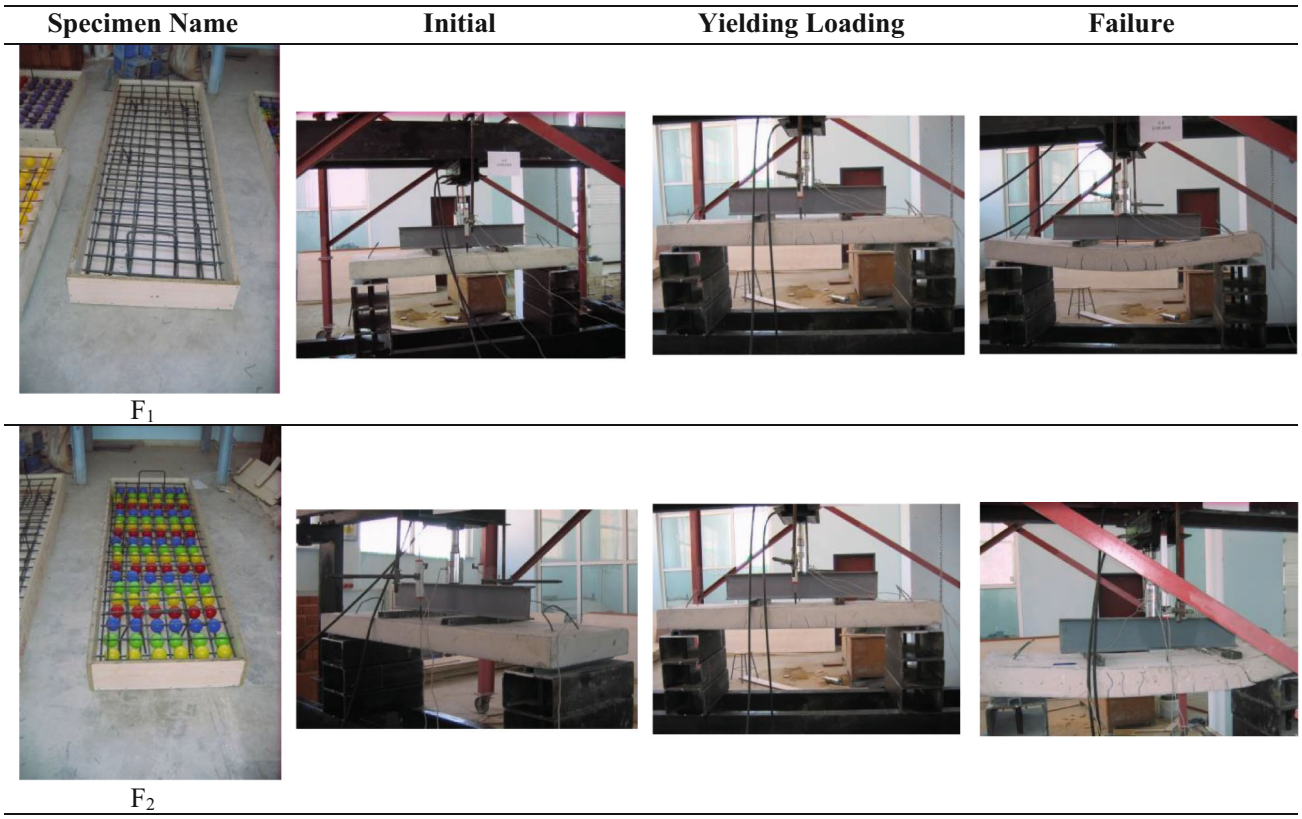

Fig. 4 Initial, yielding and ultimate conditions of the test samples

Table 3 The critical points (yielding, maximum loading, failure) of the tests

Sample	Stage						Ductility	Energy dissipated (kN-mm)
	Yielding		Maximum load		Failure			
	Load (kN) P_y	Displacement (mm) δ_y	Load (kN) P_{max}	Displacement (mm) δ_{max}	Load (kN) P_u	Displacement (mm) δ_u		
F_1	63.94	11.03	86.24	76.27	85.11	78.05	7.07	5612
F_2	62.75	10.94	81.13	81.13	83.25	82.13	7.41	5915

without balls were equivalent, and using balls did not change the capacity. The cracks observed in typical bending elements occurred under the neutral axis of the section, and after the reinforcement yielded, the crack expanded, the neutral axis was directed upwards, and damage occurred in the compression region near the end of the test. A similar crack profile occurred in both samples. The test sample conditions in different stages, such as initial, yielding, and failure, are given in Fig. 4. The values of the tests obtained at the critical points (yielding, maximum loading, and failure) are given in Table 3. As can be seen in the table, there was a 2% change in the load-carrying capacity at the time of yield, and this value reached 6% at the time of ultimate failure. This can also be explained by the faster displacement of the neutral axis after yielding. The fact that the ductility value increased by 4.8% in the balled slab can be explained as the facilitation of the voids' plastic hinge formation. Similarly, the increase in energy consumption capacity was 5.3%.

4 Numerical Study of Slab Loading

The numerical part of this study was designed to conduct a comprehensive parametric assessment. In the previous experimental part of the study, two specimens were

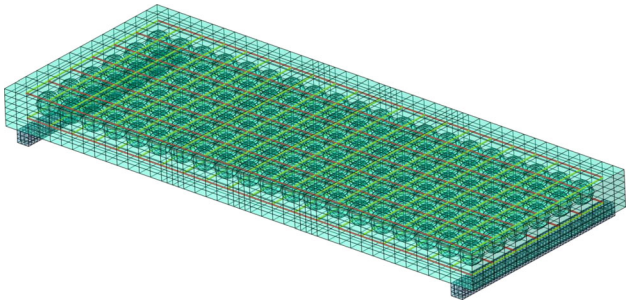

Fig. 5 Mesh configuration

exposed to vertical loading. One had no balls and one had 60 mm (D/H = 0.4) balls. The parametric study was performed to examine the effects of ball diameter, concrete class, and reinforcement ratio. Pursuant to this goal, 24 numerical models were created using finite element tools in ABAQUS.

Three-dimensional elements were used for all members. The concrete 8-node linear brick elements with reduced integration (C3D8R) were selected, while 2-node truss elements (T3D2) were used for the reinforcements. Figure 5 illustrates the mesh configuration selected for this study. The height of the slab was divided into six elements to capture the failures accurately.

Frictional interactions were defined between the supports and slab. A friction coefficient of 0.7 was selected based upon the recommendation of [42, 43]. Fixed boundary conditions were defined at the bottom of the supports, and the loads were applied to the surfaces where the loading beam contacts the slabs.

The concrete's material properties were defined using the concrete plastic damage model (CPDM), which was implemented already in the ABAQUS library. Two types of primary failure modes were defined in CDPM, tensile cracking and compressive crushing. The parameters used in the CDPM analyses are given in Table 4.

in which ψ is the dilation angle, ε is the flow potential eccentricity, σ_{b0}/σ_{c0} is the ratio of the initial equi-bi-axial compressive yield stress to initial uniaxial compressive yield stress, K is the ratio that determines the yield surface's shape, and μ is the viscosity parameter.

To obtain the tensile and compressive stress–strain curves of concrete and the elasticity modulus as well, the constitutive model of concrete Dere [44] proposed was adopted in this study. This model's accuracy was proven in the authors' previous studies [45–48]. The relation between compressive strain and compressive stress is given in Eq. 1:

$$\frac{\sigma_c}{f_c} = \frac{n\left(\frac{\varepsilon_c}{\varepsilon_{co}}\right)}{(n-1)+\left(\frac{\varepsilon_c}{\varepsilon_{co}}\right)^n}. \tag{1}$$

in which σ_c is compressive stress, ε_c is compressive strain,f_c is uniaxial compressive strength, and ε_{co} is uniaxial compressive strain. n is obtained following Eq. 2:

$$n = 0.058 f_c + 1.0. \tag{2}$$

Tensile behavior can be divided into two types. The first is elastic linear behavior, which corresponds to the ultimate tensile strength, and the behavior in the second stage is plastic. The tensile stress and strain relation is defined by Eqs. 3 and 4 as follows:

$$\sigma_t = f_t\left(\frac{\varepsilon_{to}}{\varepsilon_t}\right)^{0.4}. \tag{3}$$

in which

$$\varepsilon_{to} = \frac{f_t}{E_c}. \tag{4}$$

in which E_c is the slope of the initial tangent of the compressive stress and strain curve. Poisson's ratio of concrete is taken as 0.2, and the concrete's density was ignored. The damage in CDPM is characterized by the two main variables, d_c and d_t. The concrete compression damage parameter (d_c) and concrete tension damage parameter (d_t) were obtained with Eqs. 5 and 6:

Compression damage parameter:

$$d_c = 1 - \frac{\sigma_c E_c^{-1}}{\varepsilon_c^{pl}(1/b_c - 1) + \sigma_c E_c^{-1}}. \tag{5}$$

Tension damage parameter:

$$d_t = 1 - \frac{\sigma_t E_c^{-1}}{\varepsilon_t^{pl}(1/b_t - 1) + \sigma_t E_c^{-1}}. \tag{6}$$

The numerical results were verified using the experimental findings. Figure 6 compares the experimental and numerical findings with respect to load–displacement curves. Numerical models are able to mimic the specimens' ductile behavior accurately. Moreover, the initial and post stiffness of the experimental results was captured successfully. An approximately 1% difference in maximum load was detected between the numerical and experimental results. Thus, it can be concluded that the numerical models simulated the behavior of the specimens with and without balls accurately. After this stage, a set of parametric studies on vertical loading slabs was conducted.

Table 4 Concrete damage plasticity parameters

ψ	ε	σ_{b0}/σ_{c0}	K	μ
31	0.1	1.16	0.667	0.0005

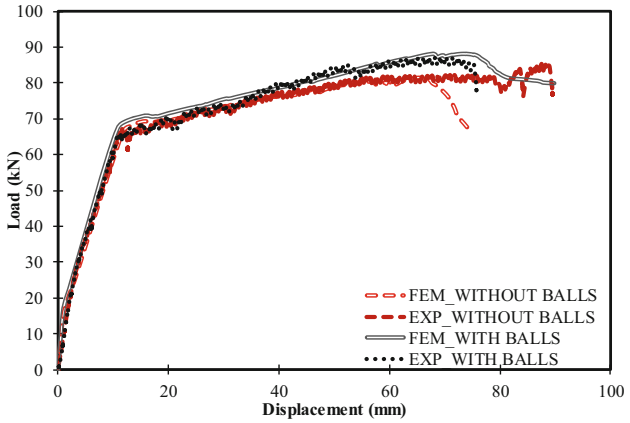

Fig. 6 Comparison of the numerical and experimental results

4.1 The Effects of Ball Diameter (*D*/*H*)

Four numerical models were developed to investigate the ball diameters' effects on the slabs' behavior. Ball diameters of 30 (*D*/*H* = 0.2), 60 (*D*/*H* = 0.4), 90 (*D*/*H* = 0.6), and 120 mm (*D*/*H* = 0.8) were selected. The slabs are depicted in Fig. 7, respectively. For this case, the concrete class remained C25 and the longitudinal reinforcement ratio remained 0.06, the same as in the experimented specimens. Figure 8 compares these numerical models' load–displacement curves. It can be seen that the models with ball diameters of 30 and 60 mm showed ductile behavior. On the other hand, the ductility decreased significantly when the ball diameter increased from 60 to 90 mm. Further, the decrease in ductility was more pronounced in the models with a ball diameter of 120 mm.

The failure modes that occurred in the numerical models with different ball diameters are shown in Fig. 9. DAMAGET (d*t*) was used to represent damage that occurred in the slabs. DAMAGET = 1 indicates that the concrete is damaged fully under tension, while

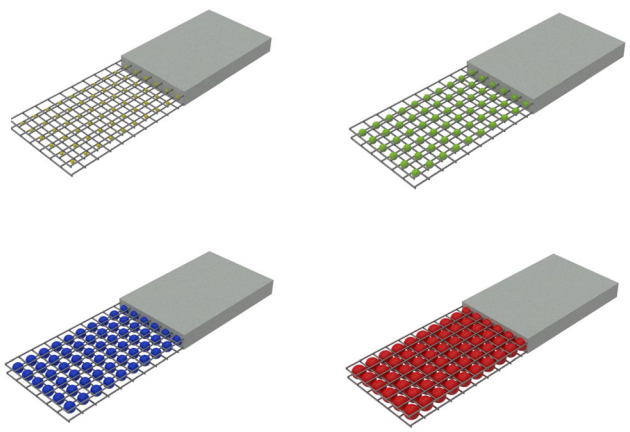

Fig. 7 The Slabs Having Different Sizes of Plastic Balls ((*D*/*H* = 0.2), (*D*/*H* = 0.4), (*D*/*H* = 0.6) mm (*D*/*H* = 0.8))

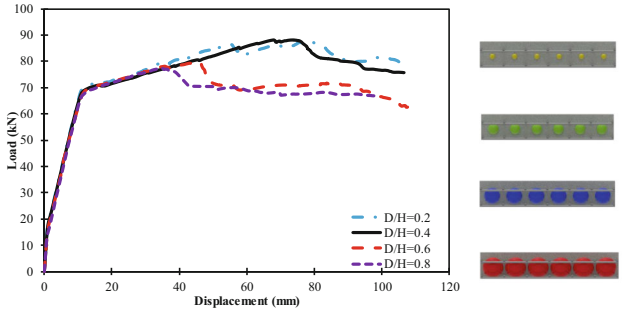

Fig. 8 The effects of ball diameter

DAMAGET = 0 indicates that no tension damage occurred. It can be seen that bending cracks were more pronounced as the *D*/*H* ratio decreased. Moreover, the damage progressed toward the supports as the *D*/*H* ratio increased.

Depending upon the load–displacement values obtained from the slabs, each sample's ductility value was also obtained. In the load–displacement curve, the yield (δ_y) and ultimate (δ_u) displacement values corresponding to 85% P_{max} were determined as considered in the literature [49–51]. Then, the ductility coefficient (μ) was calculated according to the ratio δ_u/δ_y. The ductility values obtained are given in Table 5.

4.2 The Effects of Concrete Grades

A total of 12 numerical models are compared in Fig. 10 to examine the concrete grades' effects. Concrete grades of C20, C25, and C30 [characteristic cylinder compressive strength of concrete (f_{ck}) were 20, 25 and 30 MPa, respectively], which are preferred frequently in current practice, were selected. The concrete grades were the main variable, while the *D*/*H* ratios of 0.2, 0.4, 0.6, and 0.8 were selected as a secondary variable. The results revealed that the models with C20 and C25 exhibited similar performance in load–displacement. On the other hand, the models with C30 exhibited slightly better performance than the other two. The initial stiffness increased as the concrete compressive strength increased. Depending upon the load–displacement values obtained from the slabs, each sample's ductility value was also obtained, and the values calculated are given in Table 6. These values show the change in ductility depending upon the concrete's strength, in which higher ductility values were obtained for concrete types with higher-than-average strength.

4.3 The Effects of Longitudinal Reinforcement Ratios

A total of 12 numerical models were used to investigate the longitudinal reinforcements' effects. The longitudinal

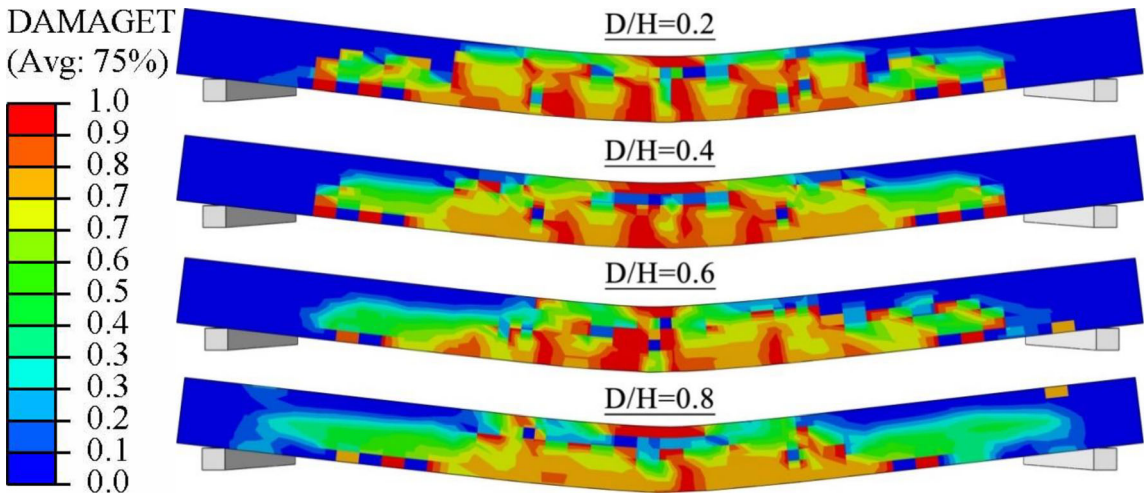

Fig. 9 Failure modes

Table 5 Ductility values obtained from FEM

D/*H* ratio	Concrete grades (MPa)	Longitudinal reinforcement ratio	δ_y (mm)	δ_u (mm)	Ductility ratio (δ_u/δ_y)
0.2	25	0.006	16.9	105.1	6.21
0.4	25	0.006	16.9	94.5	5.59
0.6	25	0.006	16.9	47.2	2.79
0.8	25	0.006	16.9	41.3	2.44

reinforcement ratios of ρ = 0.006, 0.008, and 0.01 were selected as the main variable, while *D*/*H* of 0.2, 0.4, 0.6, and 0.8 were selected as a secondary variable. Figure 11 compares the numerical values of different longitudinal reinforcement ratios. A general trend was observed, in that as the longitudinal reinforcement ratio increased, the slab's capacity increased regardless of ball diameter. However, increasing the longitudinal reinforcement ratio decreased the ductility of the numerical models with *D*/*H* = 0.8 significantly. It is obvious that increasing the reinforcement

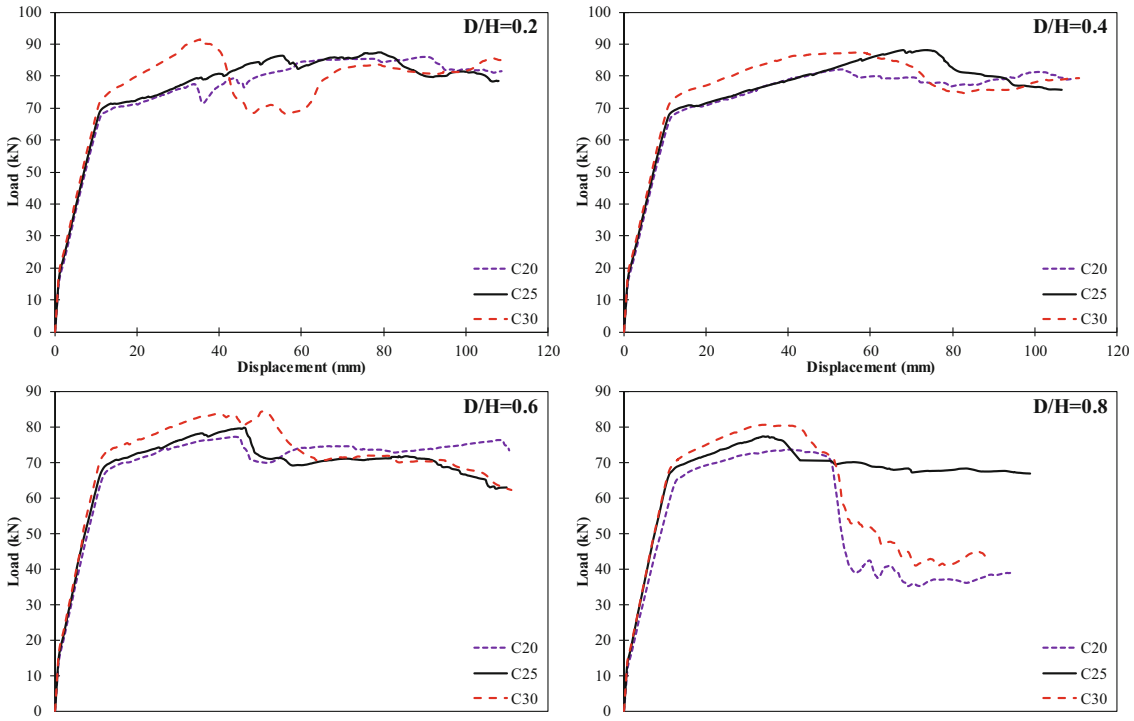

Fig. 10 The effects of the concrete grades

Table 6 Ductility values obtained from FEM

D/*H* ratio	Concrete grades (MPa)	Longitudinal reinforcement ratio	δ_y (mm)	δ_u (mm)	Ductility ratio (δ_u/δ_y)
0.2	20	0.006	17.1	111.3	6.51
0.4	20	0.006	17.0	63.2	3.71
0.6	20	0.006	17.1	49.3	2.88
0.8	20	0.006	18.4	56.3	3.06
				Average	4.04
0.2	25	0.006	16.9	105.1	6.21
0.4	25	0.006	16.9	94.5	5.59
0.6	25	0.006	16.9	47.2	2.79
0.8	25	0.006	16.9	41.3	2.44
				Average	4.25
0.2	30	0.006	15.4	43.2	6.92
0.4	30	0.006	17.1	79.2	4.63
0.6	30	0.006	16.8	61.3	3.64
0.8	30	0.006	16.9	51.2	3.03
				Average	4.55

ratio increases the strength. However, the evaluations of ductility showed that the increase in the longitudinal reinforcement in the samples with $D/H = 0.8$ reduced the section's ductility significantly. Although the increase in the reinforcement ratio is a factor that reduces the ductility in a section under the effect of bending, an almost brittle behavior was observed in the section with $D/H = 0.8$ because of the decrease in the concrete section.

Figure 12 shows further the behavior of the models with a D/H of 0.8 and different longitudinal reinforcement ratios. It can be seen that as the longitudinal reinforcement ratio increased, the cracking and failure shifted from bending to shear. For the model with $\rho = 0.01$, the shear cracks were expressed more than the bending cracks. This is observed from the fact that the damage begins to spread in the support area along with the span and its angle changes from 90° to 45°.

Depending upon the load–displacement values obtained from the slabs, each sample's ductility value was also obtained, and the values are given in Table 7.

5 Thermal and Acoustic Tests

In addition to the behavior of slabs with and without balls under vertical loads, the variation in thermal and acoustic performance depending upon ball diameters was investigated with experimental and comprehensive FEM models. In this section, the experimental and FEM analysis results

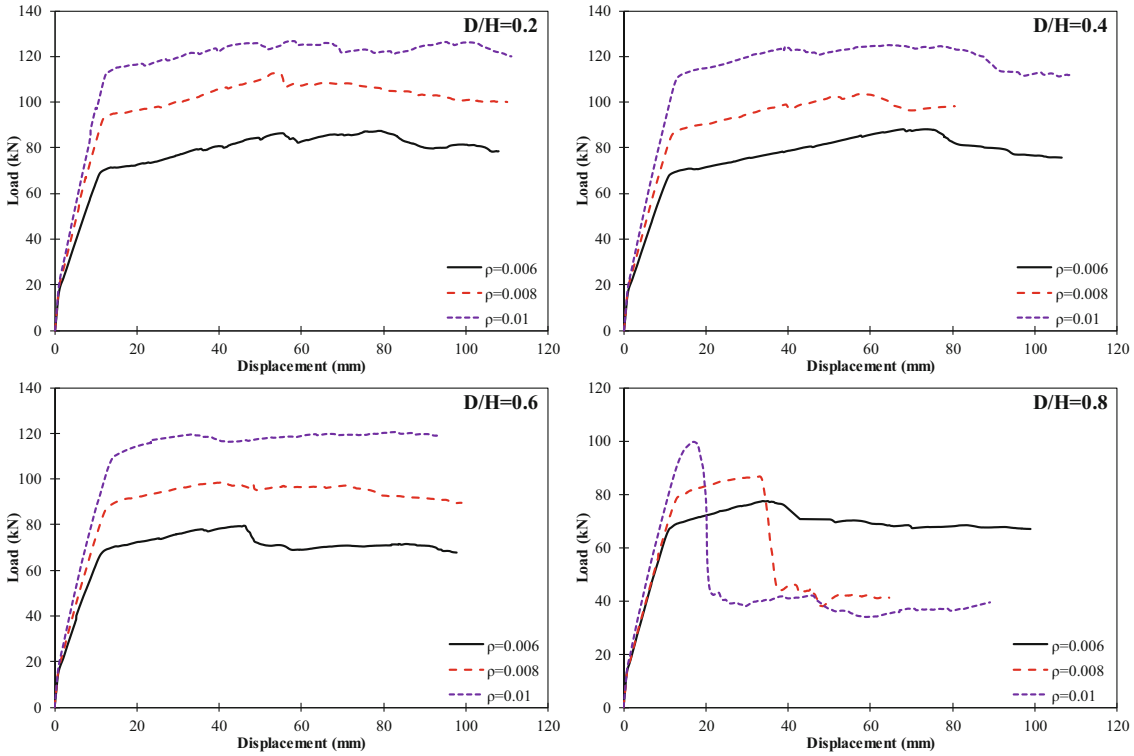

Fig. 11 The effects of the longitudinal reinforcement ratio

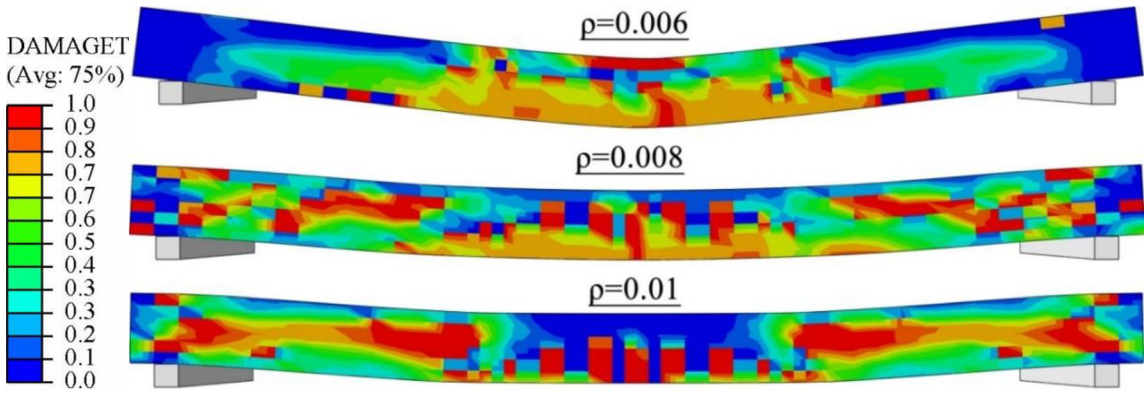

Fig. 12 The failure modes of the models with *D*/*H* of 0.8

Table 7 Ductility values obtained from FEM

D/H ratio	Concrete grades (MPa)	Longitudinal reinforcement ratio	δ_y (mm)	δ_u (mm)	Ductility ratio (δ_u/δ_y)
0.2	25	0.006	16.9	105.1	6.21
0.4	25	0.006	16.9	94.5	5.59
0.6	25	0.006	16.9	47.2	2.79
0.8	25	0.006	16.9	41.3	2.44
0.2	25	0.008	17.3	85.4	4.93
0.4	25	0.008	17.1	63.2	3.69
0.6	25	0.008	17.2	91.3	5.31
0.8	25	0.008	18.4	37.6	2.04
0.2	25	0.010	17.9	112.1	6.26
0.4	25	0.010	17.4	97.8	5.62
0.6	25	0.010	17.6	96.5	5.48
0.8	25	0.010	18.5	21.0	1.14

related to thermal and acoustic performance are interpreted based upon balls of different diameters, similar to the parametric study on vertical loading.

Before the analyses, a sensitivity analysis has been performed and it is concluded that the geometry of the wall should be divided into 2.8 million to 3 million depending on the ball size. After the mesh generation, the quality of the elements has been checked and it is seen that approximately 93% of the elements have aspect ratio between 1 and 2, while the aspect ratios of the rest of the elements vary between 2 and 3. It is concluded that these aspect ratios are sufficient for a reliable analysis.

5.1 Experimental Study of Slabs' Thermal Performance

This part of the experimental study was designed to determine the circular spacers' effects on thermal permeability. As in vertical loading, elements (M_1 and M_2) with a concrete compressive strength of approximately 26 MPa, 150 mm thickness, and 1200/1200 mm size were produced.

The experiments were carried out with the test apparatus stipulated in TS EN ISO 8990 [52] or the ASTM C-1363 [53] standards. The hot box method is one that includes the determination of thermal conductivity and heat permeability resistance in homogeneous test samples prepared in the form of masonry with a test device that consists of an insulated box divided into two parts, a hot room and cold room. The literature [54] has shown that thermal conductivity (k) (W/mK) is the most important parameter in thermal performance. All factors the affect the compressive strength and void ratio in concrete influence thermal conductivity as well. The comparative graph of the heat transfer in the samples is shown in Fig. 13. In this figure, T_h and T_c represent the temperatures of the hot and cold sides of the wall, while T_1 and T_2 represent the temperatures measured through the wall.

Table 8 shows the thermal parameters (thermal conductivity (k) W/mK, thermal conductance (C) W/m^{2}K, thermal transmittance (U) W/m^{2}K, and rate of heat (power) (Q) W), respectively. As the table indicates, mass per

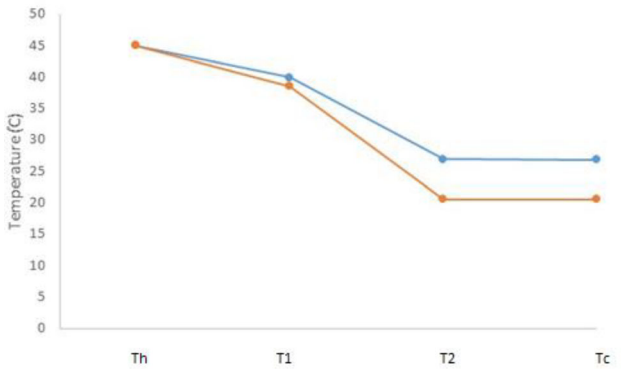

Fig. 13 Thermal transmittance of samples

Table 8 Heat transmission coefficients of specimens

Parameter	M_1	M_2	M_1/M_2
Thermal conductivity (k), W/mK	1.974	0.626	3.153
Thermal conductance (C), W/m^{2}K	13.715	2.607	5.261
Thermal transmittance (U), W/m^{2}K	9.822	1.817	5.406
Rate of heat (power) (Q), W	14.047	3.071	4.574
Mass per volume, kg/m^3	2257	1024	2.21

volume (kg/m^3) is an important parameter that affects the heat transmission coefficients. In the codes [55, 56], thermal conductivity (k) is given between 2.5 W/mK and 1.1 W/mK according to mass per volume of concrete.

5.2 Numerical Study of Slabs' Thermal Performance

The heat conduction of the RC material that contained balls of various sizes was modeled with the finite element method using ANSYS software. As in the experimental studies, both sides of the slab were exposed to constant temperatures of 45 °C and 22 °C, respectively, in the theoretical study. The area in which the plastic balls were located was modeled with an equivalent diameter and amount of air in them. Thermal models were created for both steady-state and transient heat transfer.

Figure 14 shows the variation in average slab temperature and heat flux across the slab with respect to ball diameter under the steady-state condition. As the figure illustrates, the average surface temperature and heat flux on the slab where the heat transfer takes place decreased as the ball diameters increased (ball diameters of 30 (D/H = 0.2), 60 (D/H = 0.4), 90 (D/H = 0.6), and 115 mm (D/H = 0.8)). However, it is clear that the model created is insufficient for balls with a diameter of 115 mm and shows serious deviations. Figure 15 depicts the numerical results

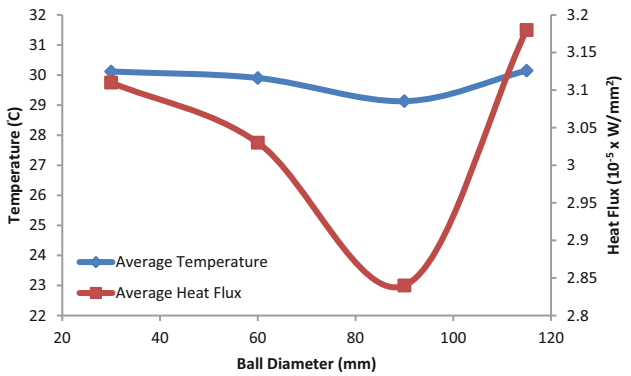

Fig. 14 Variation of average slab temperature and heat flux across the slab with respect to ball diameter under steady-state condition

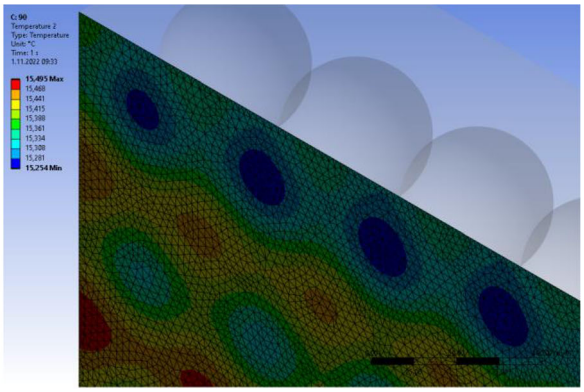

(a) Temperature distribution

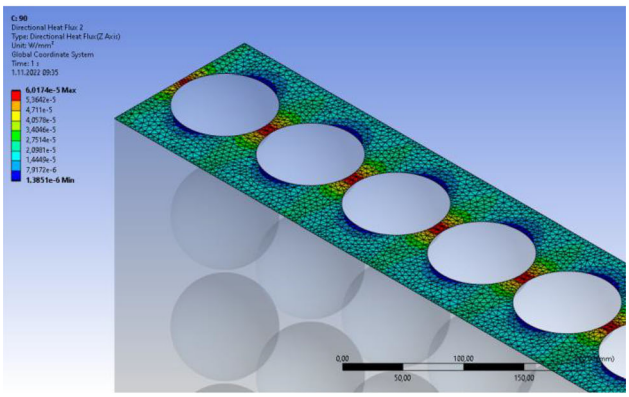

(b) Heat flux across the slab

Fig. 15 Numerical results obtained ANSYS software for ball diameter of 90 mm

Table 9 Heat conduction coefficients (W/m C)

Ball diameter (mm)	Heat conduction coefficients (W/m C)
30	1.352
60	1.317
90	1.235
115	1.383

obtained with ANSYS for a ball diameter of 90 mm. As shown in the figure, the temperature and heat flux values in the region where the balls were located differed significantly compared to the neighboring regions. Table 9 shows the equivalent heat conduction coefficients, while Fig. 16 shows the variation in the average slab temperature for different ball diameters under transient conditions. As seen in the figure, in the case of a ball diameter of 30 mm, the equilibrium temperature is higher than in other cases, but the time required for the system to stabilize is longer. This can be explained by the fact that the transient heat transfer

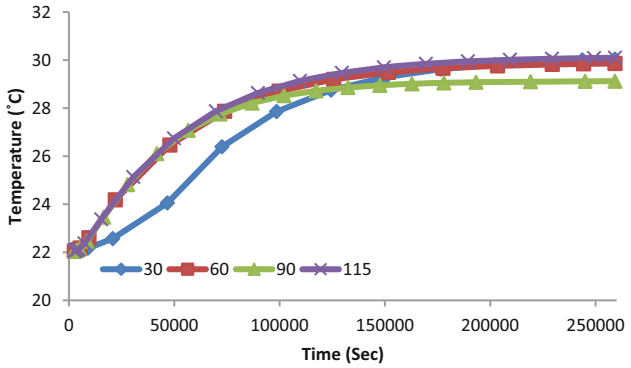

Fig. 16 Variation of average wall temperature for different ball diameters under transient condition

depends not only upon the heat conduction coefficient, but also on the material density and specific heat. Because the balls are included in the geometry, the system's equivalent density and specific heat will change.

5.3 Experimental Study of Slabs' Acoustic Performance

To perform the acoustic test, the test samples (M_1 and M_2) were produced with and without balls. The RC slab thickness used was 150 mm, the balls were 60 mm in diameter (D/H = 0.4), and the concrete elements' compressive strength was 26 MPa. In the experiments, the intensity of the sound at a certain frequency given from one side of the RC member was measured when it reached the other side of the member. The frequency range used was 100 to 3150 Hz, as in the literature [57]. The M_1 and M_2 samples' sound absorption properties are illustrated in Fig. 17. As can be seen, M_2's sound absorption values were found to be 34–43% higher at varying levels compared to those of M_1. According to the acoustic tests, the specimens' average values were 52.75 and 73.25 dB, respectively. Sound transmission properties must be known, particularly in buildings that need to provide acoustic comfort. To do so, classifications based upon transmission levels have been included in various codes, such as [58]. Sound transmission levels vary depending upon the type and thickness of the material used. In this context, M_2 performs better.

5.4 Numerical Study of Slabs' Acoustic Performance

Acoustic analyses were performed with ANSYS finite element software. A mass source of 2.10^{-7} kg/mm^2 s was applied from one surface of the modeled wall and the sound level on the other side of the wall was measured in dBA. The RC wall's acoustic properties were modeled using the Miki model [59]. The concrete wall's fluid resistivity value and the speed of sound in air were chosen as 8000 kg/m^{3}s and 346.25 m/s, respectively. Figure 18 show the acoustic performance of slabs with plastic balls of different diameters. As seen in these figures, the sound

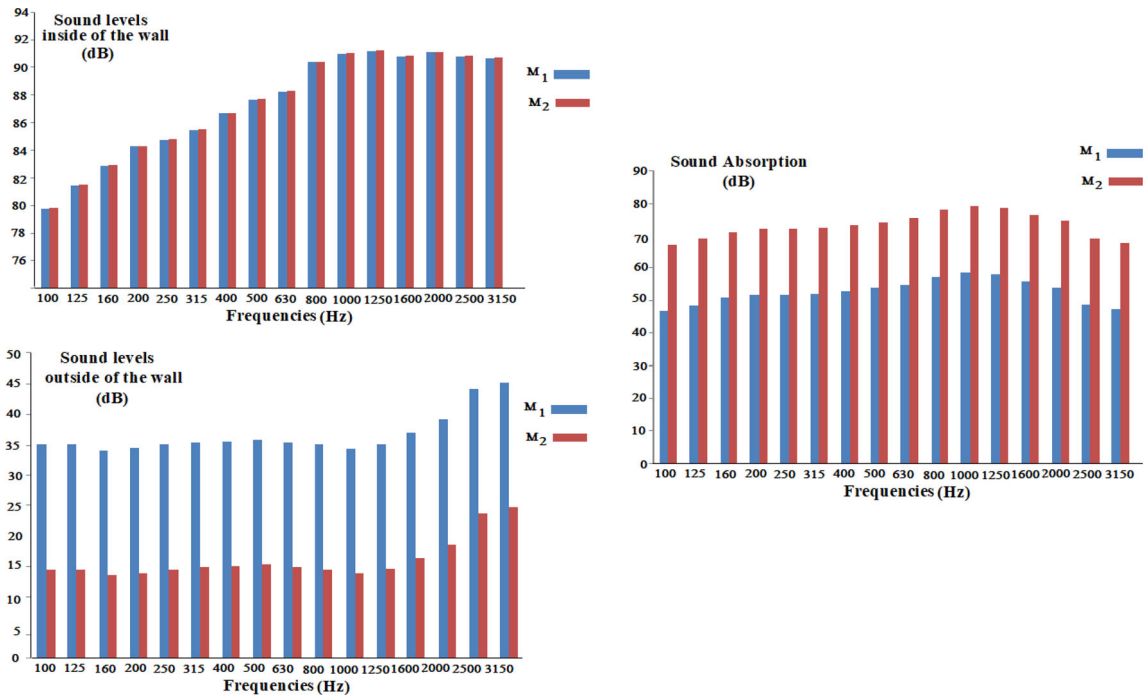

Fig. 17 Measured sound levels for different frequencies in M_1 and M_2

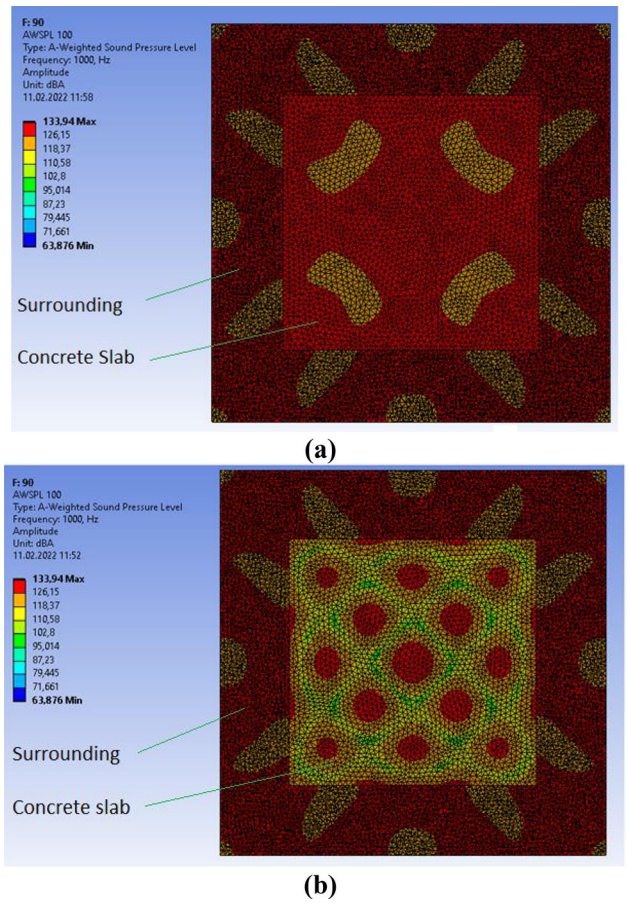

Fig. 18 Sound pressure levels of concrete slab with balls (sound frequency 1000 Hz, ball diameter 90 mm), **a** sound incoming direction, **b** sound outgoing direction

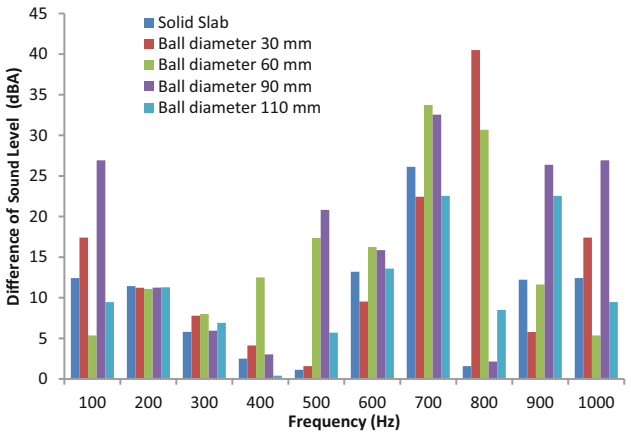

Fig. 19 Variation of sound pressure level for different ball diameters

level the slabs absorbed varied depending upon both the diameter of the balls used and the frequency. In Fig. 19, it is seen that sound was dampened in the range of 0.5–40 dBA depending upon the frequency. In this situation, it is understood that walls with balls of different diameters can be selected according to sound sources with a certain frequency.

6 Results and Discussion

In this study, the effect of plastic balls placed within RC slabs to create spaces was investigated with respect to different engineering problems. Most importantly, the study determined whether the placement of balls changed the behavior of slabs under vertical loading. To do so, an experimental study was conducted, and then the experimental results were verified with advanced FEM software. Further, a parametric study was carried out after the results obtained from the FEM converged with the experimental results at a high estimation capacity. In addition to the behavior of slabs with and without balls under vertical loads, the variation in thermal and acoustic performance depending upon ball diameters was investigated experimentally and with comprehensive FEM models. The findings obtained from the study are as follows:

1) According to the results of the experimental study, when a 60 mm ball is used in slabs 150 cm thick ($D/H = 0.4$), the slabs' vertical load-carrying capacity decreased by 1.8% when the longitudinal reinforcement of the slab yielded. In the ultimate state in which the load-carrying capacity is reached, this decrease was 6.02%.
2) The slabs' ductility increased by 4.8% when balls were used. In RC members, the slabs' curvature and ductility value reached 7.41, as the slabs are exposed to the effect of bending to a large extent and the reinforcement chosen was under-balanced. The energy absorption capacity increased by 5.4% in proportion to the slabs' ductility ratio.
3) According to the FEM model, when the D/H ratio was 0.2 and 0.4, the results were very similar. However, if the D/H ratio chosen was 0.6 and 0.8, the load-carrying capacities at the time the reinforcement yielded longitudinally did not change, but because the concrete area in the compression zone decreased, the specimens could not deform too much and showed ductile behavior after yielding. The results also showed that bending cracks were more pronounced as the D/H ratio decreased. Moreover, the damage progressed toward the supports as the D/H ratio increases.
4) While the variation that depended upon diameter was limited in the C20 and C25 grade concretes, the increase in load-carrying capacity was more evident in C30 class concretes, in which the initial stiffness

increased as the concrete's compressive strength increased.

5) A general trend was observed in the FEM results, in that as the longitudinal reinforcement ratio increased, the slab's capacity increased regardless of ball diameter. However, increasing the longitudinal reinforcement ratio decreased the ductility of the numerical models with $D/H = 0.8$ significantly.
6) The heat and sound coefficients obtained and calculated from the heat and sound experiments performed varied considerably. While the sound absorption value increased by 37% when plastic balls were used, the thermal conductivity coefficient decreased by 68%.
7) In the numerical study of the slabs' thermal performance, the average surface temperature and heat flux on the slab where the heat transfer takes place decreased as the ball diameters increased. However, it is understood that the model generated was insufficient for $D/H = 0.8$ and showed serious deviations.
8) As the acoustic models show, the sound level the slabs absorbed varied depending upon both the diameter of the balls used and the frequency. It caused sound damping in the range of 0.5–40 dBA depending upon the frequency. In this situation, it is understood that walls with balls of different diameters can be selected to dampen sound sources with a certain frequency.
9) In future studies, it will be very valuable to carry out experimental and analytical studies on balled slabs' vibrational behavior. As this study demonstrated, the greatest advantage of this slab system is its lightness. However, vibration problems must be controlled even in long-term human use, particularly if the support is a simple support. In this respect, dynamic analysis and modeling will be beneficial for these slabs.

7 Conclusion

In this study, the differences that occur in load-carrying, heat, and acoustic insulation when circular cross-sectional plastic balls are used in RC slabs are described. It is useful to discuss the applicability of the study to RC buildings in the long term and the advantages it will bring.

RC is the most preferred building system in the world. Because of the increasing population and limited residential areas, multi-story RC buildings have become a mandatory choice for people. It is obvious that there will be limits in the production of concrete, which is the raw material of RC buildings' carrier systems, in the near future. The European Green Deal's [60, 61] objective is to reduce carbon emissions between 2030 and 2050 with certain innovations in the use of concrete (hence the use of cement and aggregate). In RC buildings, slab elements constitute a significant part of a building's RC mass. If circular voids can be created within the slabs and selected and placed properly, concrete use can be reduced substantially without significant loss of load-bearing capacity. Based upon the D/H ratios tested in this study, if a ratio of 0.4 (with no significant reduction in load-carrying capacity) is selected, it will result in a 32% reduction in the amount of concrete used. In addition to the decrease in the dead loads on the building's structural system, there will be a slight decrease in the inertia force that will protect the structure during an earthquake. Similarly, a partial reduction in foundation dimensions can be expected.

However, the most important lessons learned from past earthquakes is that because the horizontal rigidity is insufficient in buildings with flat slabs (without beams), too much displacement arises during earthquakes. In this case, non-ductile columns cause brittle damage. It would be appropriate to use balled slabs, particularly in areas where gravity-loads are active. However, if void or hollow slabs are to be used in structures built in earthquake-prone regions, they must have additional shear walls that increase the load-bearing system's global lateral rigidity.

Consideration should be given to the fact that the balls used are produced by recycling plastic material that is found as waste in nature. This will be both an environmentally responsible approach and will allow the building to be constructed more economically when the unit price of concrete and plastic materials is considered. Further, by choosing the diameters of the circular spaces appropriately, the heat and acoustic insulation properties between floors will be improved and will reduce the energy use indirectly.

Acknowledgements The author thanks Konya KOSGEB TEKMER and Scientific Research Projects (BAP) of the Selçuk University for their financial support.

Funding The funding taken for the experimental part of the study are mentioned in the acknowledgment part.

Data availability Authors can confirm that all relevant data are included in the article.

Declarations

Conflict of interest The authors confirm that there are no known conflicts of interest associated with this publication and there has been no financial support for this work that could have influenced its outcome.

Intellectual property We confirm that we have given due consideration to the protection of intellectual property associated with this work

and that there are no impediments to publication, including the timing of publication, with respect to intellectual property. In so doing, we confirm that we have followed the regulations of our institutions concerning intellectual property. We confirm that the manuscript has been read and approved by all named authors. We confirm that the order of authors listed in the manuscript has been approved by all named authors.

References

1. Dash MK, Patro SK, Rath AK (2016) Sustainable use of industrial-waste as partial replacement of fine aggregate for preparation of concrete—a review. Int J Sustain Built Environ 5(2):484–516
2. Ahmed S, Arocho I (2021) Analysis of cost comparison and effects of change orders during construction: study of a mass timber and a concrete building project. J Build Eng 33:101856
3. Sadri H, Pourbagheri P, Yitmen I (2022) Towards the implications of Boverket's climate declaration act for sustainability indices in the Swedish construction industry. Build Environ 207:108446
4. Alonso A, Suárez R, Patricio J, Escandón R, Sendra JJ (2021) Acoustic retrofit strategies of windows in facades of residential buildings: Requirements and recommendations to reduce exposure to environmental noise. J Build Eng 41:102773
5. Neya I, Yamegueu D, Coulibaly Y, Messan A, Ouedraogo ALSN (2021) Impact of insulation and wall thickness in compressed earth buildings in hot and dry tropical regions. J Build Eng 33:101612
6. Alonso A, Patricio J, Suárez R, Escandón R (2020) Acoustical retrofit of existing residential buildings: requirements and recommendations for sound insulation between dwellings in Europe and other countries worldwide. Build Environ 174:106771
7. Gong L, Chen Z, Feng Y, Ruan S, Tu L (2021) Experimental study on an innovative hollow concrete floor system assembled with precast panels and self-thermal-insulation infills. Adv Civ Eng 2021:6663412
8. Fediuk R, Amran M, Vatin N, Vasilev Y, Lesovik V, Ozbakkaloglu T (2021) Acoustic properties of ınnovative concretes: a review. Materials 14(2):398
9. Paik I, Na S, Yoon S (2019) Assessment of CO_2 emissions by replacing an ordinary reinforced concrete slab with the void slab system in a high-rise commercial residential complex building in South Korea. Sustainability 11(1):82
10. Mohan A, Sukumaran Archana (2018) Performance analysis of bubble deck slab using elliptical balls, International journal of engineering research & technology (IJERT) ETCEA 6(6)
11. Bindea M, Zagon R, Kiss Z (2013) Flat slabs with spherical voids. Part II: experimental tests concerning shear strength. Acta Technica Napocensis Civ Eng Archit 56(1):74–81
12. Oukaili NK, Husain LF (2017) Punching shear in reinforced concrete bubbled slabs: experimental investigation. Smart monitoring, assessment and rehabilitation of civil structures, Zurich, Switzerland
13. Han SW, Lee CS (2014) Evaluation of punching shear strength of voided transfer slabs. Mag Concr Res 66(21):1116–1128
14. Teja PP, Kumar PV, Anusha S, Mounika C, Saha P (2012) Structural behavior of bubble deck slab. In: IEEE-ınternational conference on advances in engineering, science and management (ICAESM-2012), IEEE, 2012, pp. 383–388
15. Hai LV, Hung VD, Thi TM, Nguyen-Thoi T, Phuoc NT (2013) The experimental analysis of bubbledeck slab using modified elliptical balls. In: Thirteenth East Asia-Pacific conference on structural engineering and construction (EASEC-13), pp. G-6
16. Harba IS, Hammed MA (2019) Numerical analysis of shear strength behavior of self-compact reinforced concrete two-way bubble deck slab with shear reinforcement. In: IOP conference series: materials science and engineering, IOP Publishing, p. 022050
17. Kumar MV, Abou Hamza T (2020) Finite element analysis on effect of different ball spacing in bubble deck lightweight concrete slab. In: IOP conference series: materials science and engineering, IOP Publishing, p. 012124
18. Anusha M, Surendra HJ, Vinod BR, Bhavya S (2022) Modelling using finite element analysis in the structural behavior of bubble deck slab. Mater Today Proc 66:2397–2404
19. Ibrahim AM, Ali NK, Salman WD (2013) Flexural capacities of reinforced concrete two-way bubbledeck slabs of plastic spherical voids. Diyala J Eng Sci 6(2):9–20
20. Surendar M, Ranjitham M, Scholar PG (2016) Numerical and experimental study on bubble deck slab. Int J Eng Sci Comput 6(5):5959–5962
21. Shetkar A, Hanche N (2015) An experimental study on bubble deck slab system with elliptical balls. Proc NCRIET-2015 Indian J Sci 12(1):021–027
22. Chung JH, Choi HK, Lee SC, Choi CS (2011) Shear capacity of biaxial hollow slab with donut type hollow sphere. Proc Eng 14:2219–2222
23. Zafar NTS (2016) Structural behaviour of bubble deck slabs and its application: main paper IJSRD. Int J Sci Res Dev 4(2):2321–2613
24. Lai T (2010) Structural behavior of BubbleDeck® slabs and their application to lightweight bridge decks
25. Marais CC, Robberts JM, Van Rensburg BWJ (2010) Spherical void formers in concrete slabs: technical paper. J S Afr Inst Civ Eng 52(2):2–11
26. Meng Y, Ling T-C, Mo KH (2018) Recycling of wastes for value-added applications in concrete blocks: an overview. Resour Conserv Recycl 138:298–312
27. Prabhu GG, Hyun JH, Kim YY (2014) Effects of foundry sand as a fine aggregate in concrete production. Constr Build Mater 70:514–521
28. Ahmed HU, Faraj RH, Hilal N, Mohammed AA, Sherwani AFH (2021) Use of recycled fibers in concrete composites: a systematic comprehensive review. Compos B Eng 215:108769
29. Sandanayake M, Law D, Sargent P (2022) A new framework for assessing the environmental impacts of circular economy friendly soil waste-based geopolymer cements. Build Environ 210:108702
30. Chen W, Yang S, Zhang X, Jordan ND, Huang J (2022) Embodied energy and carbon emissions of building materials in China. Build Environ 207:108434
31. Shinde P, Patil M, Jadhav M, Degloorkar S (2018) Comparative study of flat plate slab and voided slab lightened with U-Boot Beton. Int Res J Eng Technol 5:3684–3686
32. Kannas H, Alhassan M, Wafi AMS (2020) Cobiax and post-tension slabs: a comparative study based on the construction duration time and cost. Int J Adv Eng Sci Appl 1(4):1–6
33. Ghalimath A, Meshram P, Singh U. U-boot void slab. Int J Innov Eng Res Technol (2019) 1–2
34. Abramski M, Albert A, Nitsch A, Schnell J. Bearing behaviour of biaxial hollow core slabs. Int Assoc Bridge Struct Eng, Presented at IABSE Symposium: Large Structures and Infrastructures for Environmentally Constrained and Urbanised Areas, Venice, Italy, 22–24 September 2010, 23–30
35. Polak MA (ed) (2005) Punching shear in reinforced concrete slabs. American Concrete Institute. SP-232, symposium paper, 232, 302
36. Schnellenbach-Held M, Denk H (1999) BubbleDeck time-dependent behaviour, local punching additional experimental tests. Technische Universität Darmstadt, DACON 14, pp. 137–144

37. Mustafa SAA, Fathy E, Essa MA, Mohammed AAE (2019) Evaluation of structural performance and energy saving ability of normal, voided and foamed RC slabs. HBRC J 15(1):33–54
38. Broms CE (2000) Elimination of flat plate punching failure mode. ACI Struct J 97(1):94–101
39. Oukaili NK, Husain LF (2016) Punching shear strength of bubbledecks under eccentric loads. In Proceeding of SecondInternational Conference on Science, Engineering and Environment pp 222–227
40. Harba ISI, Hameed MA (2018) Shear behavior of self compacted reinforced concrete two way bubble slabs. Int J Civ Eng Technol (IJCIET) 9(12):1117–1127
41. Requirements for design and consctruction of reinforced concrete structures. Turkish Building Code, TBC-500-2000, Ankara (2020)
42. Aksoylu C, Özkılıç YO, Arslan MH (2020) Damages on prefabricated concrete dapped-end purlins due to snow loads and a novel reinforcement detail. Eng Struct 225:111225
43. Özkılıç YO, Aksoylu C, Arslan MH (2021) Experimental and numerical investigations of steel fiber reinforced concrete dapped-end purlins. J Build Eng 36:102119
44. Dere Y (2017) Assessing a retrofitting method for existing RC buildings with low seismic capacity in Turkey. J Perform Constr Facil 31(2):04016098
45. Özkılıç YO, Yazman Ş, Aksoylu C, Arslan MH, Gemi L (2021) Numerical investigation of the parameters influencing the behavior of dapped end prefabricated concrete purlins with and without CFRP strengthening. Constr Build Mater 275:122173
46. Aksoylu C, Özkılıç YO, Yazman Ş, Gemi L, Arslan MH (2021) Experimental and numerical ınvestigation of load bearing capacity of thinned end precast purlin beams and solution proposals. Teknik Dergi
47. Özkılıç YO, Aksoylu C, Arslan MH (2021) Numerical evaluation of effects of shear span, stirrup spacing and angle of stirrup on reinforced concrete beam behaviour. Struct Eng Mech Int J 79(3):309–326
48. Gemi L, Madenci E, Özkılıç YO (2021) Experimental, analytical and numerical investigation of pultruded GFRP composite beams infilled with hybrid FRP reinforced concrete. Eng Struct 244:112790
49. Aksoylu C, Özkılıç YO, Arslan MH (2022) Mechanical steel stitches: an innovative approach for strengthening shear deficiency in undamaged reinforced concrete beams. Buildings 12(10):1501
50. Karalar M, Özkılıç YO, Deifalla AF, Aksoylu C, Arslan MH, Ahmad M, Sabri MMS (2022) Improvement in bending performance of reinforced concrete beams produced with waste lathe scraps. Sustainability 14(19):12660
51. Aksoylu C, Özkılıç YO, Hadzima-Nyarko M, Işık E, Arslan MH (2022) Investigation on improvement in shear performance of reinforced-concrete beams produced with recycled steel wires from waste tires. Sustainability 14(20):13360
52. S. International Organization for (1994) Thermal ınsulation: determination of steady-state thermal transmission properties: calibrated and guarded hot box, ınternational organization for standardization
53. American Society for, D.o.T.I. Materials (2011) Committee, Standard test method for thermal performance of building materials and envelope assemblies by means of a hot box apparatus. ASTM International, West Conshohocken
54. Kim K-H, Jeon S-E, Kim J-K, Yang S (2003) An experimental study on thermal conductivity of concrete. Cem Concr Res 33(3):363–371
55. ASTM C1045:2007 (2007) Standard practice for calculating thermal transmission properties under steady-state conditions. ASTM International, West Conshohocken
56. DIN Deutsches Institut für Normung e.V. DIN EN 15643-2:2011-05 Nachhaltigkeit von Bauwerken—Bewertung der Nachhaltigkeit von Gebäuden—Teil 2: Rahmenbedingungen für die Bewertung der Umweltbezogenen Qualität; Sustainability of Construction Works—Assessment of Buildings—Part 2: Framework for the Assessment of Environmental Performance; (DIN EN 15643-2); Beuth Verlag GmbH: Berlin, Germany, 2015.
57. Binici H, Aksogan O, Bakbak D, Kaplan H, Isik B (2009) Sound insulation of fibre reinforced mud brick walls. Constr Build Mater 23(2):1035–1041
58. Garg N, Sharma O, Maji S (2011) Design considerations of building elements for traffic and aircraft noise abatement
59. Miki Y (1990) Acoustical properties of porous materials-Modifications of Delany-Bazley models. J Acoust Soc Jpn (E) 11(1):19–24
60. European Commission (2019) The European green deal. Eur Commun 53:24
61. Assembly G (2012) Resolution adopted by the General Assembly on 27 July 2012. United Nations, Norfolk